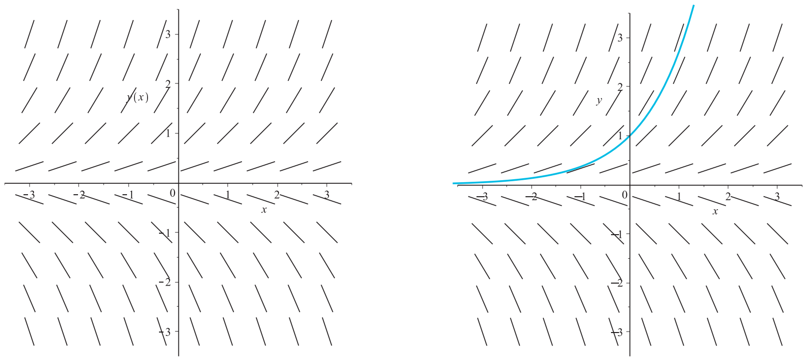


**(a)** **(b)**

Figure 2.1 The direction field for $\frac{dy}{dx} = y$ is shown in **(a)**. The graph of $y(x)$ through the point (0, 1) on the direction field for $\frac{dy}{dx} = y$ is shown in **(b)**.

002x001.eps

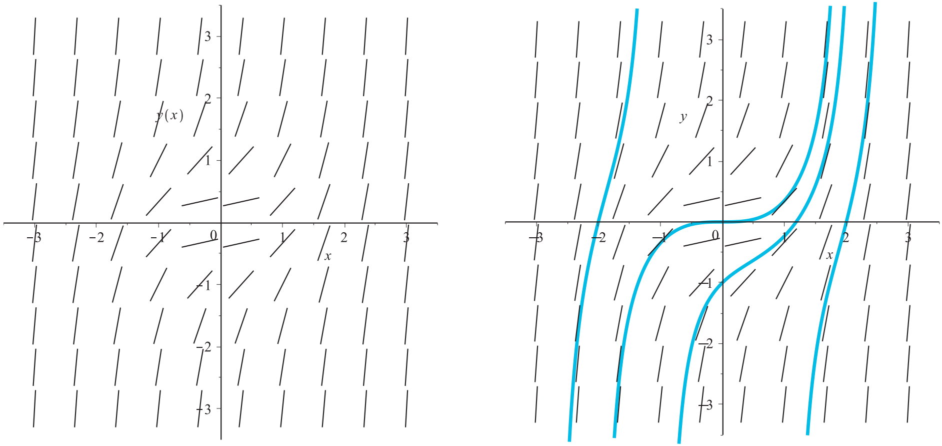


**(a)** **(b)**

Figure 2.2 The direction field for $\frac{dy}{dx} = x^2 + y^2$ is shown in **(a)**. Graphs of several solutions $y(x)$ on the direction field for $\frac{dy}{dx} = x^2 + y^2$ are shown in **(b)**.

002x002.eps

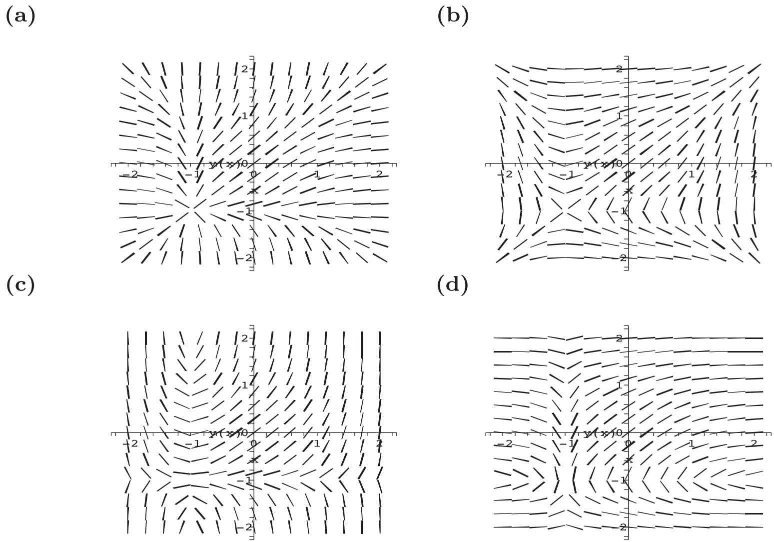


Figure 2.3  Direction fields for Problems **1–4**.

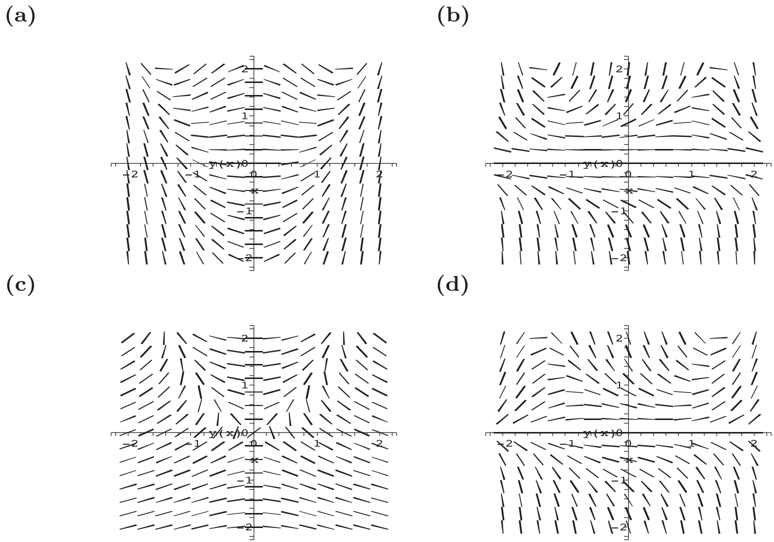


Figure 2.4 Direction fields for Problems **5–8**.

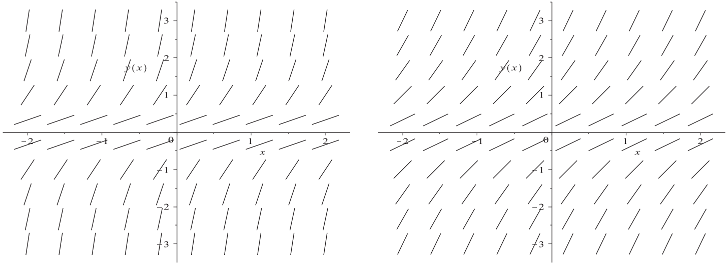


**(a)** **(b)**

Figure 2.5 Direction fields for (a) $y' = 3y^{4/3}$ and (b) $y' = 2y^{2/3}$.

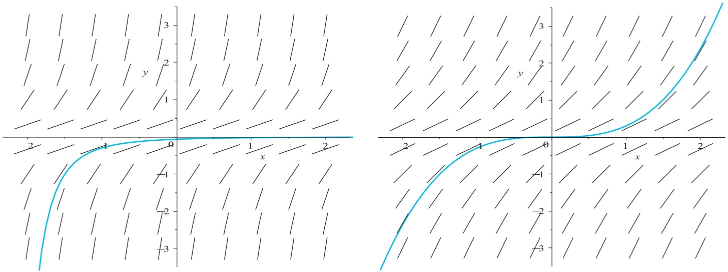


(a) (b)

Figure 2.6 Direction fields for (a) $y' = 3y^{4/3}$ with IC $y(\frac{-3}{2}) = -1$, which stays in bottom half plane and (b) $y' = 2y^{2/3}$ with IC $y(\frac{-3}{2}) = -1$, which passes through upper half plane.

002x006.eps

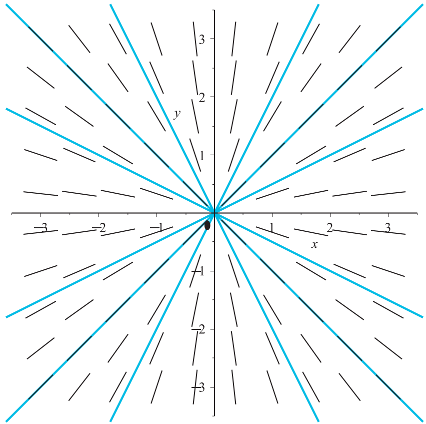


Figure 2.7 Direction fields for $\frac{dy}{dx} = \frac{y}{x}$. Note that all the solutions shown here satisfy the initial condition $y(0) = 0$.

002x007.eps

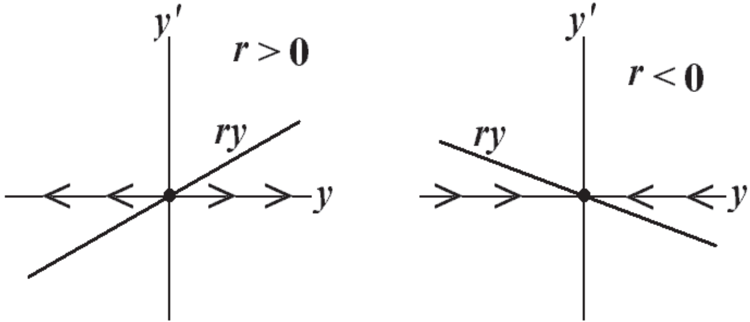


Figure 2.8 Phase line diagrams for Equation (2.4).

002x008.eps

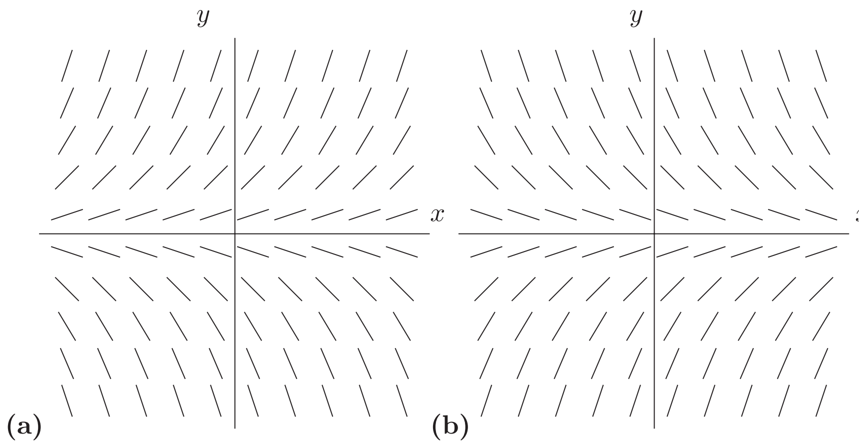


Figure 2.9 The $y$-$y'$ direction field for $\frac{dy}{dx} = ry$ . In **(a)**, we have $r > 0$ and in **(b)** we have $r < 0$.

002x009.eps

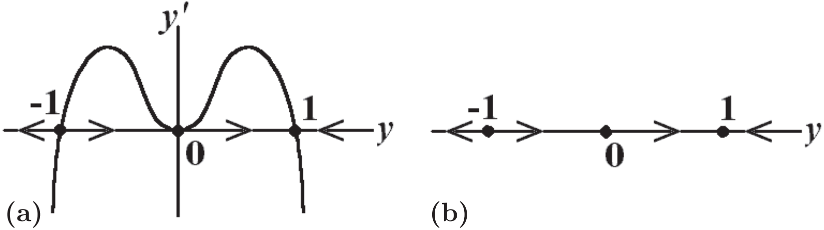


Figure 2.10 View of (2.5) in the (a) $y$-$y'$ plane and (b) phase line.

002x010.eps

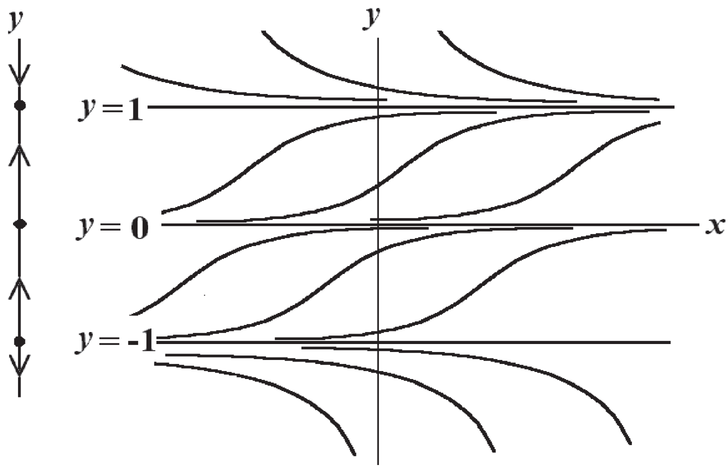


Figure 2.11 Sketch of some solutions of (2.5), based exclusively on phase line information; phase line (on left) from Figure 2.10 is now drawn vertically for easier comparison.

002x011.eps

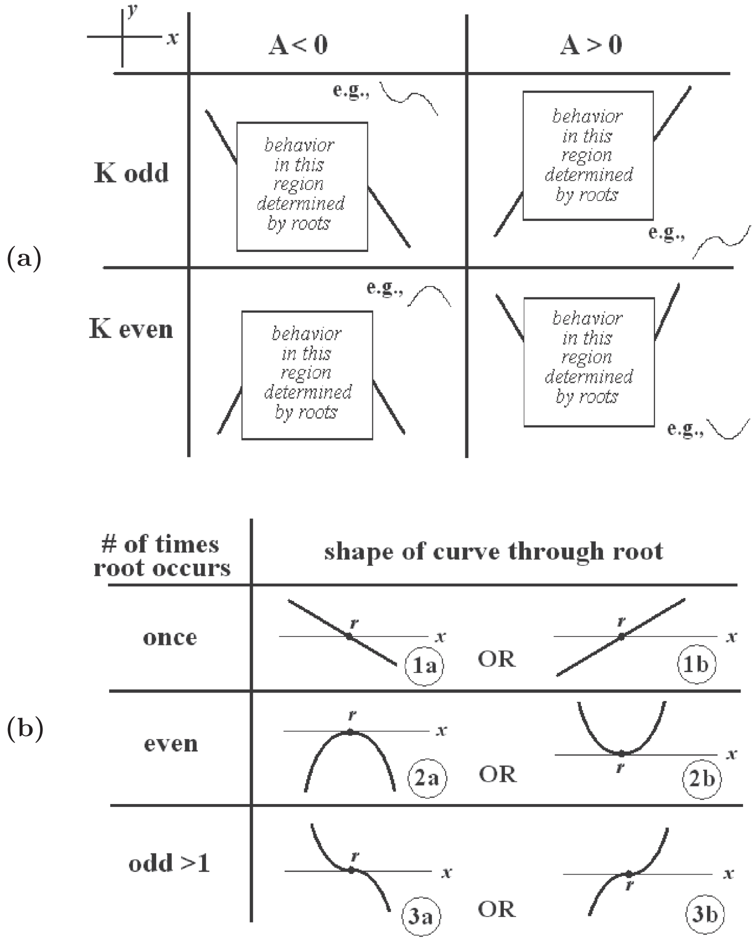


Figure 2.12 (a) Behavior of factored polynomial (2.8) for large $|x|$. The curves obey $\lim_{x\to-\infty} P(x)$ and $\lim_{x\to\infty} P(x)$ . (b) Behavior near the roots of factored polynomial (2.8).

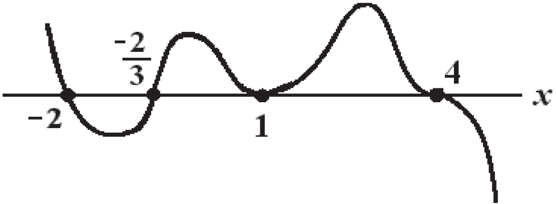


Figure 2.13 Sketch of $P(x) = (x-1)^2(2+3x)(4-x)^3(x+2)$.

002x013.eps

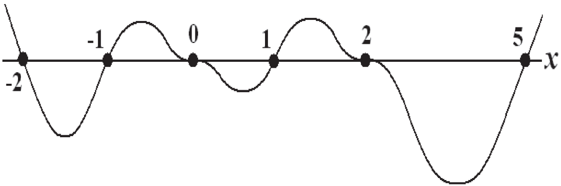


Figure 2.14 Sketch of $P(x) = -x^3(x^2-4)(x-1)(5-x)(3+3x)(4-2x)^2(x^2+1)$.

002x014.eps

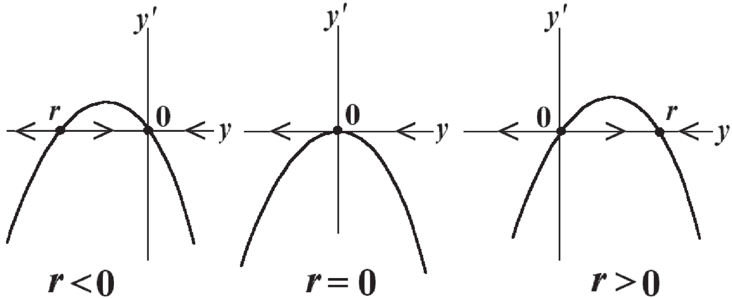


Figure 2.15 Phase line view of a transcritical bifurcation. The bifurcation happens at the value $r = 0$ but we determine the type of bifurcation by observing what happens before (for $r < 0$) and after (for $r > 0$).

002x015.eps

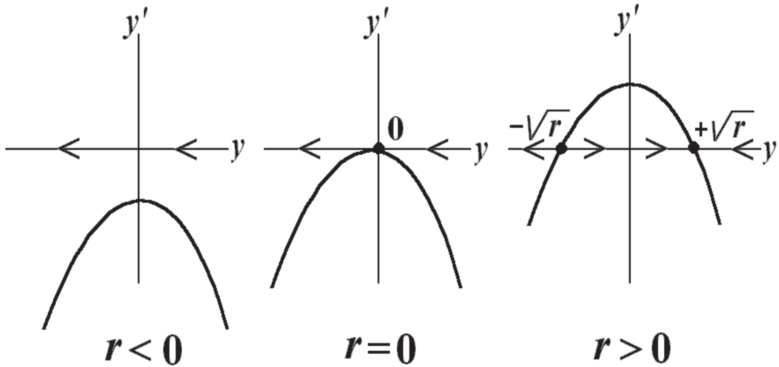


Figure 2.16 Phase line view of a saddlenode bifurcation. The bifurcation happens at the value $r = 0$ but we determine the type of bifurcation by observing what happens before (for $r < 0$) and after (for $r > 0$).

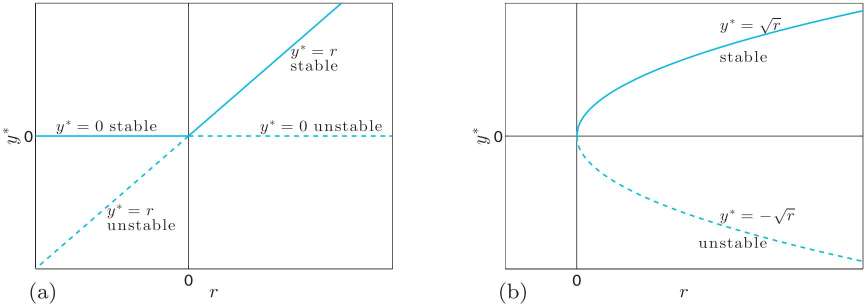


Figure 2.17 (a) Transcritical bifurcation diagram. Equilibria curves obtained from Figure 2.15. (b) Saddlenode bifurcation diagram. Equilibria curves obtained from Figure 2.16.

002x017.eps

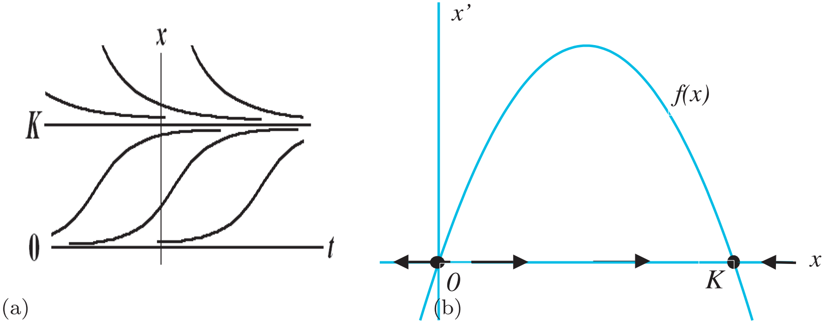


Figure 2.18 (a) Qualitative behavior of the solutions to the logistic equation. (b) Phase line for the logistic equation.

002x018.eps

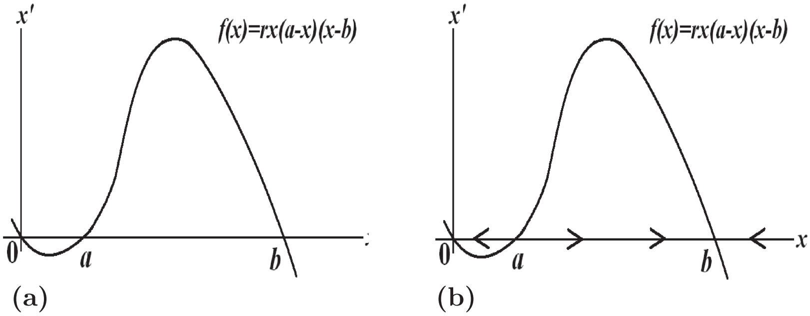


Figure 2.19 (a) Cubic from Allee effect model. (b) Phase line diagram for Allee effect model.

002x019.eps

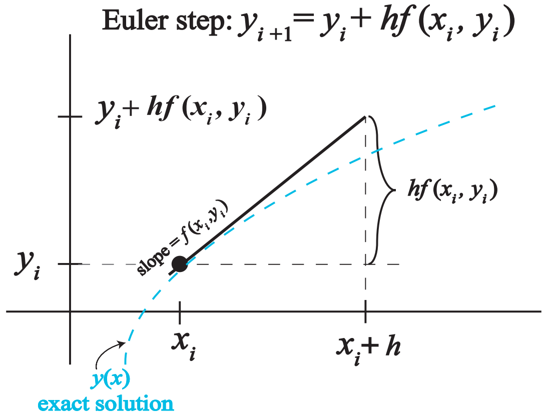


Figure 2.20 One step of Euler's method. Given the point $(x_i, y_i)$, the next $y$-value is calculated by $y_{i+1} = y_i + hf(x_i, y_i)$: Note that no information regarding the function on the interval $(x_i, x_i + h)$ is used to calculate the approximation at $x_i + h$.

002x020.eps

| $x_i$ | $y_i$ | $x_i$ | $y_i$ |
|---|---|---|---|
| 0.0 | 1.0 | 0.6 | 1.15873 |
| 0.1 | 1.0 | 0.7 | 1.22825 |
| 0.2 | 1.01 | 0.8 | 1.31423 |
| 0.3 | 1.0302 | 0.9 | 1.41937 |
| 0.4 | 1.06111 | 1.0 | 1.54711 |
| 0.5 | 1.10355 | | |

Figure 2.21 Euler's method with $h = 0.1$ for the equation $\frac{dy}{dx} = xy$.

002x021.eps

| $x_i$ | Euler $y_i$ | Exact $y(x_i)$ | Error $\lvert y_i - y(x_i)\rvert$ |
|---|---|---|---|
| 0.0 | 1.0 | 1.0 | 0 |
| 0.1 | 1.0 | 1.0050 | 0.005 |
| 0.2 | 1.01 | 1.0202 | 0.0102 |
| 0.3 | 1.0302 | 1.0460 | 0.0158 |
| 0.4 | 1.06111 | 1.08329 | 0.02218 |
| 0.5 | 1.10355 | 1.13315 | 0.02960 |
| 0.6 | 1.15873 | 1.19722 | 0.03849 |
| 0.7 | 1.22825 | 1.27762 | 0.04937 |
| 0.8 | 1.31423 | 1.37713 | 0.06290 |
| 0.9 | 1.41937 | 1.49930 | 0.07993 |
| 1.0 | 1.54711 | 1.64872 | 0.10161 |

Figure 2.22 Euler's method with $h = 0.1$ compared with the exact solution for the equation $\frac{dy}{dx} = xy$.

002x022.eps

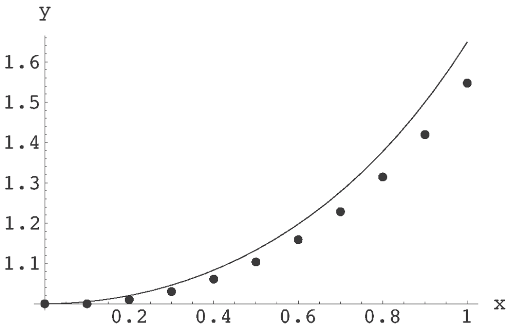


Figure 2.23 Plot of $y(x) = e^{x^2/2}$ with points obtained via Euler's method.

002x023.eps

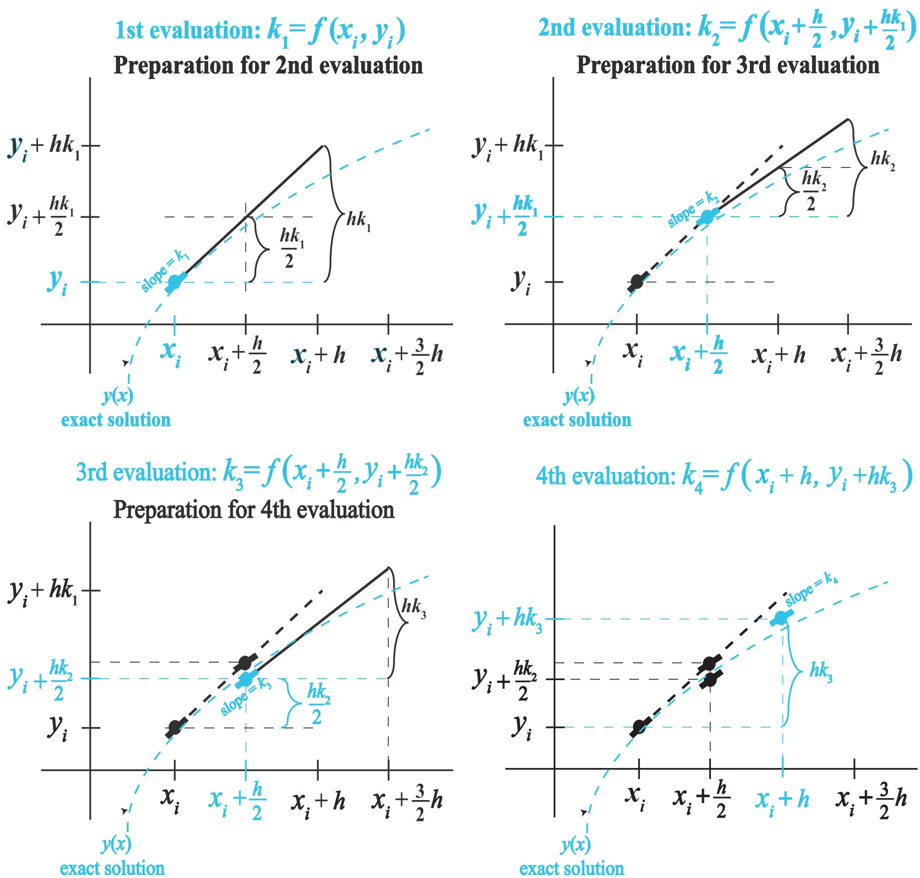


Figure 2.24 One step of fourth-order Runge-Kutta. Given the point $(x_i, y_i)$, the next $y$-value is calculated by $y_{i+1} = y_i + h(k_1 + 2k_2 + 2k_3 + k_4)/6$. The graph here is shown for a solution that is increasing and concave down on the interval $(x_i, x_i + h)$.

| $x_i$ | Runge-Kutta $y_i$ | True $y(x_i)$ | Error $\|y_i - y(x_i)\|$ |
|---|---|---|---|
| 0.0 | 1.0 | 1.0 | 0.0 |
| 0.1 | 1.0050125 | 1.0050125 | 0.0000000 |
| 0.2 | 1.0202013 | 1.0202013 | 0.0000000 |
| 0.3 | 1.0460279 | 1.0460279 | 0.0000000 |
| 0.4 | 1.0832871 | 1.0832872 | 0.0000000 |
| 0.5 | 1.1331485 | 1.1331484 | 0.0000001 |
| 0.6 | 1.1972174 | 1.1972173 | 0.0000001 |
| 0.7 | 1.2776213 | 1.2776213 | 0.0000000 |
| 0.8 | 1.3771278 | 1.3771277 | 0.0000001 |
| 0.9 | 1.4993025 | 1.4993024 | 0.0000001 |
| 1.0 | 1.6487213 | 1.6487210 | 0.0000003 |

Figure 2.25 Runge-Kutta's method with $h = 0.1$ compared with the analytic solution ($e^{x^2/2}$) for the equation $\frac{dy}{dx} = xy$ .

002x025.eps

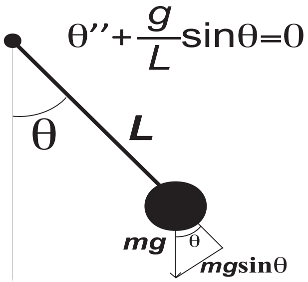


Figure 2.26  Free body diagram for simple pendulum without friction.

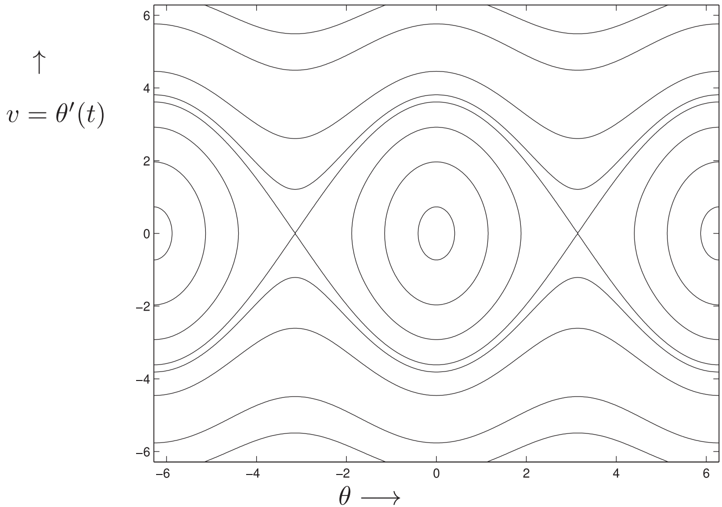


Figure 2.27 Orbits for simple pendulum with $g = 9{:}8$, $L = 1$:

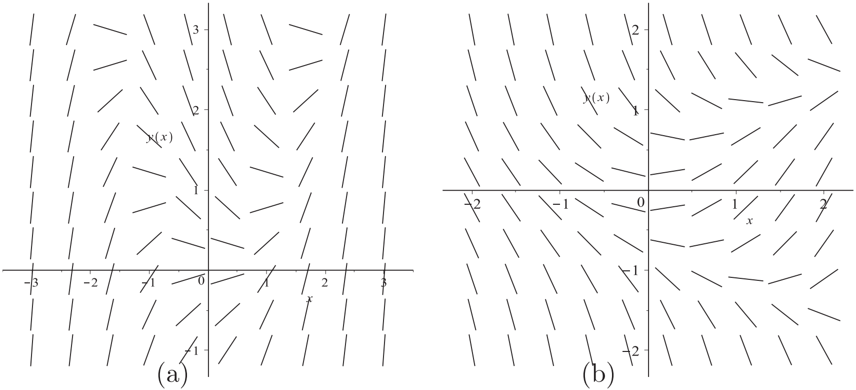


Figure 2.28 (a) Graph for Problem **14**. (b) Graph for Problem **15**.

002x028.eps

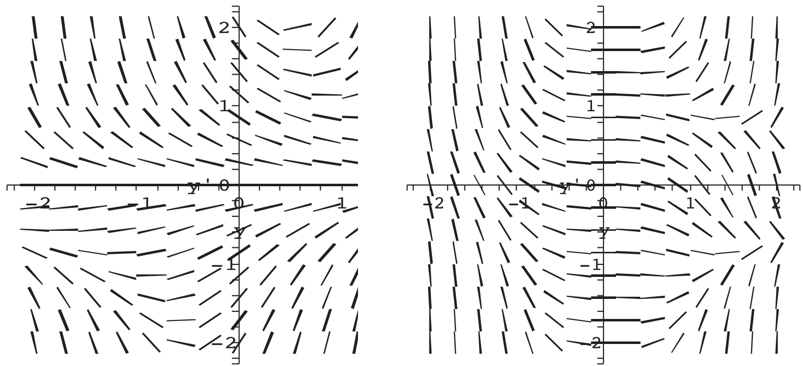


Figure 2.29 Direction fields for Problem **19**.

Courtesy of CRC Press/Taylor & Francis Group

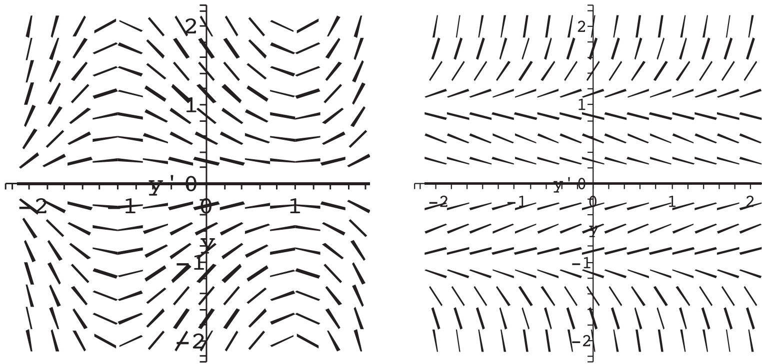


Figure 2.30 Direction fields for Problem **20**.

002x030.eps

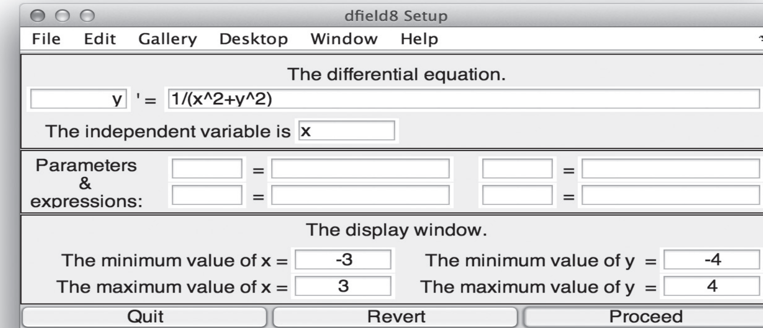


Figure 2.31 Pop-up window for dfield8 program, used to obtain numerical solutions to first-order equations.

002x031.eps